Applied Energy 205 (2017) 892–902

Contents lists available at ScienceDirect

Applied Energy

journal homepage: www.elsevier.com/locate/apenergy

A study on the impact of open circuit voltage tests on state of charge estimation for lithium-ion batteries

Cheng Lin[a], Quanqing Yu[a,b], Rui Xiong[a,*], Le Yi Wang[b]

[a] Collaborative Innovation Center of Electric Vehicles in Beijing, School of Mechanical Engineering, Beijing Institute of Technology, Beijing 100081, China
[b] Department of Electrical and Computer Engineering, Wayne State University, Detroit, MI 48202, USA

HIGHLIGHTS

- Two common tests for observing OCV performance of NMC and LFP cells are studied.
- The temperature, age and relaxation time dependency of the OCV-SoC is investigated.
- A parameters and state of charge joint estimation method is presented.
- The proposed joint estimation method is verified in terms of accuracy and robustness.
- The incremental OCV test is recommended to determine the OCV-SoC relationship.

ARTICLE INFO

Keywords:
State of charge
Lithium ion batteries
H_∞ filter
Open circuit voltage
Incremental OCV test
Low current OCV test

ABSTRACT

The open circuit voltage (OCV) is of essential importance for accurate estimation of the state of charge (SoC) in lithium-ion battery (LiB). The OCV-SoC relationship is typically predetermined by fitting offline OCV data. Commonly used two OCV tests are compared in few literatures. Moreover, they only focus on the middle SoC region (i.e., 20% and 90%) of $LiNiMnCoO_2$ (NMC) LiBs, the performances of these OCV tests for other battery types and entire SoC region are failed to be addressed. In this paper, the impact of two OCV tests on SoC estimation for NMC and $LiFePO_4$ (LFP) LiBs is investigated at different temperatures and aging stages. A parameter and SoC joint estimation method is introduced, based on an integrated H_∞-UKF method. The accuracy and reliability of the proposed method are verified by using two different OCV testing data at various ambient temperatures and aging stages for some commercial NMC and LFP LiBs. The results indicate that the incremental OCV test method results in more accurate SoC estimation than the low current OCV test method, on both NMC and LFP LiBs. Furthermore, to reach equilibrium states and achieve desired SoC estimation accuracy, the relaxation period in the incremental OCV test method needs to be extended at low temperatures.

1. Introduction

Electric vehicles (EVs) have gained popularity in recent years, for their inherent environmental benefits of reduced gas emissions. Battery systems and their management are the most critical technology supporting EV market penetration. Among various battery types, lithium-ion batteries (LiBs) such as $LiNiMnCoO_2$ (NMC) and $LiFePO_4$ (LFP) LiBs are widely used in EVs due to their high energy and power densities [1,2]. To ensure safe, reliable, and sustained operations of battery systems, a high-performance battery management system (BMS) needs to be developed to monitor and control the states of batteries [3], in which the most important one is the SoC [4]. Many approaches have been proposed for estimating the SoC [5–9]; and most of them are model-based [10,11]. In model-based SoC estimation, the battery model typically consists of a linear dynamic state equation and a highly nonlinear OCV-SoC function in its output equation. The accuracy of both equations is essential for SoC estimation, but this paper is devoted to the impact of OCV-SOC functions predetermined by different OCV tests on SoC estimation accuracy.

Since the SoC cannot be directly measured, it must be estimated or inferred from measured signals. Compared with the complicated electrochemical models [12,13], equivalent circuit models (ECMs) can represent empirical behaviours of battery systems with much fewer parameters and have been employed in a wide range of applications [14]. For ECMs, parameter identification of the model is the foundation of battery SoC estimation. Commonly used methods are the least

* Corresponding author at: Department of Vehicle Engineering, School of Mechanical Engineering, Beijing Institute of Technology, No. 5 South Zhongguancun Street, Haidian District, Beijing 100081, China.
E-mail address: rxiong@bit.edu.cn (R. Xiong).

http://dx.doi.org/10.1016/j.apenergy.2017.08.124
Received 27 May 2017; Received in revised form 24 July 2017; Accepted 12 August 2017
Available online 20 August 2017
0306-2619/

Nomenclature

OCV	open circuit voltage
SoC	state of charge
NMC	$LiNiMnCoO_2$ batteries
LFP	$LiFePO_4$ batteries
IO	incremental OCV test
LO	low-current OCV test
DST	dynamic stress test
UDDS	Urban Dynamometer Driving Schedule
EV	electric vehicle
ECM	equivalent circuit model
U_t	terminal voltage
U_p	polarization voltage
i_o	current
R_o	ohmic resistance
R_p	polarization resistance
C_p	polarization capacitance
C_n	maximum available capacity
η_i	charge or discharge efficiency
Δt	sampling interval
s	abbreviation of SoC

squares (LS) approach [15–17] and recursive LS (RLS) estimation [1,18–20]. By using the identified parameters in the battery models, Kalman filters (KFs) and extended KFs (EKFs) are often used to estimate the SoC of battery [4,21–24]. Furthermore, unscented KFs (UKFs) and H_∞ filters have also been employed to improve the accuracy of SoC estimation [25–28].

In applying this parameter and state estimation method, the OCV is an indispensable variable to SoC estimation and which needs to be estimated accurately [1,10,22,29–31]. The OCV is commonly treated as a nonlinear function of SoC [32], and the relationship between the OCV and SoC varies with ambient temperature [24,33,34], aging stages [33,35] and relaxation time [36,37]. Currently, there are two commonly used OCV test methods to determine the relationship between battery OCV and SoC, the incremental OCV (IO) test [36,38–40] and the low current OCV (LO) test [10,34,41]. Zheng, et al. [42] firstly studied the influence of these two OCV test methods on SoC online estimation of NMC cells at different temperatures. However, there remain several open issues. First, two sets of static parameters were identified by the LS method by using DST data at a certain temperature without considering the influence of real operating conditions and temperatures on them, which resulted in large SoC error occurs under different dynamic tests and low temperatures. So, it's not reasonable to observe the impact of different OCV tests on SoC online estimation with inaccurate SoC results. Second, the study only focuses on the SoC region between 10% and 90%, however, considering the difficulty in obtaining the accurate SoC initial value in the real application, the two OCV tests should be compared in entire SoC region. Third, relaxation time affects the OCV-SoC curve. Using a constant relaxation time for incremental OCV tests at different temperatures is not reasonable. Fourth, LFP cells are also commonly used in EVs. Unlike NMC cells, the OCV-SoC curves of LFP cells typically have a wide flat range of SoC in middle SoC region and change dramatically in low and high SoC regions. As a result. Therefore, the performances of different OCV tests for different battery types are should be further investigated.

The contributions of this paper are as follows: (1) The impact of two traditional OCV test methods for online SoC estimation considering different battery types are studied under different ambient temperatures, aging stages, and entire SoC region. (2) An H_∞-UKF joint SoC estimation method is employed to update parameters and states in real-time. The OCV model only affects the SoC estimation process other than the parameters identification process. (3) The influence of relaxation time at low temperature on the incremental OCV test method is investigated for both NMC and LFP LiBs. A recommendation on extended relaxation time is given accordingly.

The remainder of this paper is organized as follows: Section 2 introduces the battery specifications and battery model used in this paper. In Section 3, two OCV-SoC mapping tests are introduced. In addition, two OCV-SoC mapping results at various temperatures and aging stages for NMC and LFP LiBs are presented. Then an H_∞-UKF joint SoC estimation method is introduced in Section 4. The results and discussions are presented in Section 5. Finally, Section 6 concludes the paper with some discussions on potential future directions.

2. Battery model

NMC and LFP LiBs that are commonly used in EVs. The test bench in [43] is used to carry out the experiments in this study. The basic specifications of cells are given in Table 1. It should be pointed out that NMC01 is a fresh cell, whose actual capacity is 28.40 Ah at 25 °C. NMC04 is an aged cell which has undergone 400 cycle life tests (i.e., Hybrid DST-UDDS tests), whose actual capacity has decreased to 25.51 Ah at 25 °C which indicates a capacity loss of 10.2%. Similarly, LFP01 is a fresh cell, whose actual capacity is 19.84 Ah at 25 °C. and LFP09 is an aged cell which has undergone 900 cycle life tests (i.e., Hybrid DST-UDDS tests) with its actual capacity decreased to 17.77 A h at 25 °C which indicates a capacity loss of 10.5%.

The Thevenin model as shown in Fig. 1 is selected to represent the NMC and LFP LiBs due to its high estimation accuracy and low complexity. The dynamics of the battery cells can be described by Eqs. (1) and discretized to Eq. (2).

$$\begin{cases} \dot{U}_p = \frac{i_o}{C_p} - \frac{U_p}{C_p \times R_p} \\ U_t = OCV - U_p - i_o R_o \end{cases} \tag{1}$$

$$\begin{cases} U_{p,k+1} = \exp\left(-\frac{\Delta t}{C_{p,k} \times R_{p,k}}\right) U_{p,k} + \left(1 - \exp(-\frac{\Delta t}{C_{p,k} \times R_{p,k}})\right) R_p i_{o,k} \\ U_{t,k} = OCV_k - U_{p,k} - i_{o,k} R_{o,k} \end{cases} \tag{2}$$

where i_o is the current with a positive value for discharge and a negative value for charge; R_o is the ohmic resistance; R_p and C_p represent the polarization resistance and polarization capacitance, respectively; U_p is the polarization voltage across C_p while U_t denotes the terminal voltage; Δt is the sampling interval; U_{oc} is the battery OCV which can be expressed by

$$OCV = c_0 + c_1 s + c_2 s^2 + c_3 s^3 + c_4 s^4 + c_5 s^5 + c_6 s^6 + c_7 s^7 + c_8 s^8 + c_9 s^9 \tag{3}$$

$$s_k = s_{k-1} - \frac{\eta_i i_o \Delta t}{C_n} \tag{4}$$

where c_i $(i = 0, 1, \ldots, 9)$ are the parameters to fit the OCV-SoC

Table 1
Basic specifications of the battery cells.

Cell	Nominal voltage	Nominal capacity	Actual maximum available capacity (40 °C/25 °C/10 °C)	Lower/upper cutoff voltage
NMC01	3.7 V	25 A h	28.91 A h/28.40 A h/26.37 A h	2.5 V/4.2 V
NMC04	3.7 V	25 A h	25.89 A h/25.51 A h/24.77 A h	2.5 V/4.2 V
LFP01	3.2 V	20 A h	19.79 A h/19.84 A h/19.71 A h	2.0 V/3.65 V
LFP09	3.2 V	20 A h	17.67 A h/17.77 A h/17.88 A h	2.0 V/3.65 V

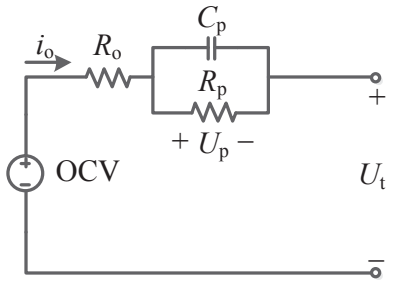

Fig. 1. Thevenin model structure.

relationship which commonly determined through the offline OCV-SoC test; s represents the battery SoC; η_i is the charge or discharge efficiency; C_n is the actual maximum available capacity of the battery, which is given in Table 1 and varies with ambient temperatures and age stages. The C-rate of cell capacity test is 0.3 C for constant current (CC) phase, at the upper cutoff voltage as shown in Table 1, a constant voltage (CV) phase is applied until the current become less than 0.05 C to ensure that the cell is fully charged.

3. OCV-SoC mapping tests

For OCV-SoC mapping tests, the SoC is calculated by ampere hour counting method which was shown as Eq. (4), and the OCV can be obtained from different OCV tests.

During the incremental OCV test, the cells should be fully charged with the same CCCV method as capacity test. Then, gradually discharged with a positive pulse current-relaxation duration in every 10% SoC step until the lower cutoff voltage is reached. It is noteworthy that the 10% SoC is calculated by ampere hour counting method and the used capacity varies with ambient temperatures and age stages. After resting for 2 h, the cells are then charged with a negative current-relaxation duration in every 10% SoC step until the upper cutoff voltage is reached. Finally, a CV phase is applied to fully charge the battery cells. At each pulse current-relaxation duration, the current is set to 0.5 C and the relaxation time is set to 2 h to eliminate the polarization effect inside the battery. The current and voltage profiles of cell LFP01 at 25 °C are given in Fig. 2(A) and (B). Finally, the set of averaged voltage data at every 10% SoC of the discharging and charging processes is fitted via Eq. (3) to obtain the OCV-SoC curve.

For the low current OCV test, the cells are discharged or charged at a constant low current rate of 0.05 C until the lower or upper cutoff voltage is reached. The current and voltage profiles of cell LFP01 at 25 °C are given in Fig. 2 (A) and (C), respectively. Finally, the set of averaged voltage data at every 10% SoC of the discharging and charging processes is fitted via Eq. (3) to obtain the OCV-SoC curve.

In this study, we investigate the impact of three ambient temperatures (10 °C, 25 °C, and 40 °C) on the OCV-SoC relationship of NMC and LFP cells. In addition, the influence of two aging stages at 10 °C on the OCV-SoC relationship of NMC and LFP cells is also studied. One reason for studying aging effect at 10 °C is that the difference between two OCV tests is obvious at low temperatures [42]. Another reason is to investigate why the SoC estimation errors are so large at low temperatures [42].

Fig. 3 shows the OCV-SoC curves of two OCV tests at different ambient temperatures and aging stages for NMC and LFP cells. It is interesting to note that the OCV-SoC curves of NMC cells are quite different from that of LFP cells. The OCV-SoC curves of NMC cells change dramatically in low SoC region while the OCV-SoC curves of LFP cells change dramatically in low and high SoC regions.

Fig. 3(A) shows the OCV-SoC curves of the incremental OCV test for NMC cells. It is observed that the OCV-SoC curves at three temperatures of the new cell NMC01 overlap in the range of 40–90% SoC. There is an obvious difference in the ranges of 0–40% and 90–100% SoC. Compared with the new cell NMC01 at 10 °C, the OCV-SoC curve of the aged cell NMC04 has negligible differences in the ranges of 65–100% and 20–35% SoC while it has an obvious difference in the ranges of 35–65% and 0–20% SoC. Unlike the incremental OCV test, the low current OCV-SoC curves as shown in Fig. 3(B) at three temperatures of the new cell NMC01 overlap almost in the whole range of SoC except for the beginning of SoC (0–10%). Compared with the new cell NMC01 at 10 °C, the OCV-SoC curve of the aged cell NMC04 has negligible differences in the ranges of 75–100% and 10–35% SoC while it has an obvious difference in the ranges of 35–70% and 0–10% SoC. Fig. 3(C) indicates the differences between the two OCV-SoC tests at different temperatures and aging stages. The curves of the two OCV tests differ significantly for the new cell NMC01 and aged cell NMC04 at low temperatures (10 °C), in comparison to the room temperature (25 °C) and high temperature

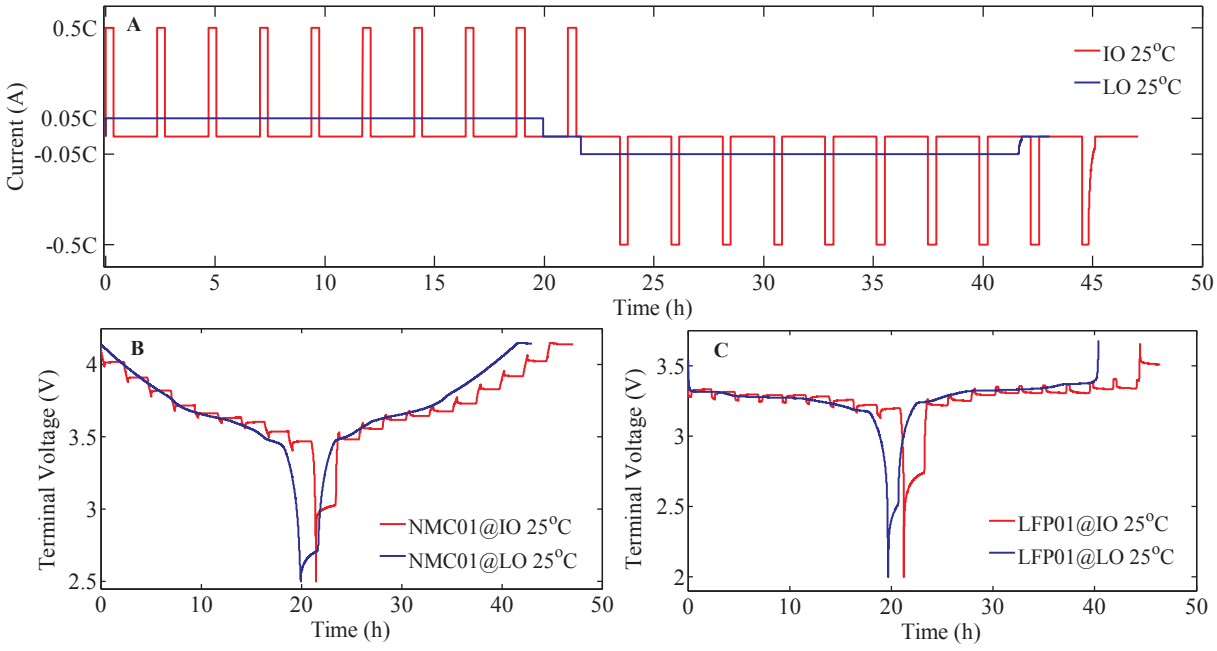

Fig. 2. Current and terminal voltage profiles of two OCV tests: (A) current profiles, (B) terminal voltage profiles of NMC01 cell, (C) terminal voltage profiles of LFP01 cell.

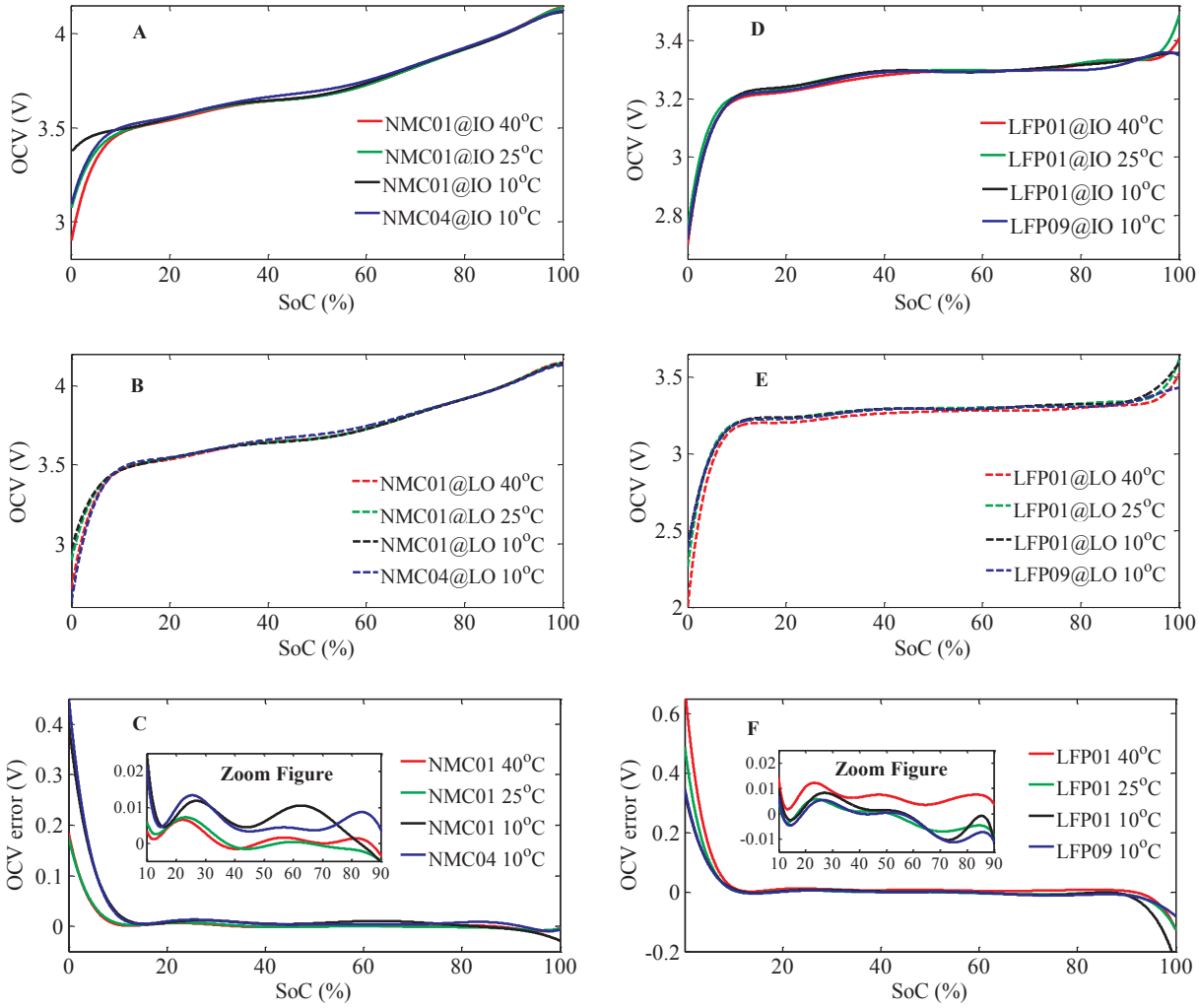

Fig. 3. OCV-SoC curves and errors of two OCV tests at different temperatures and aging stages: (A) IO test for NMC cells, (B) LO test for NMC cells, (C) OCV errors for NMC cells, (D) IO test for LFP cells, (E) LO test for LFP cells, (F) OCV errors for LFP cells.

Table 2
Summary of the H_∞ filter for the parameters identification.

- **Initialization:** for $k = 0$, set $\hat{x}^+_{h,0}, P^+_{h,0}, S_0, \theta, Q_{h,0}, R_{h,0}$
- **Time update:** for $k = 0$, calculate
  Prior estimate of state: $\hat{x}^-_{h,k} = A_{h,k-1}\hat{x}^+_{h,k-1} + B_{h,k-1}i_{o,k-1}$
  Prior estimate of covariance: $P^-_{h,k} = A_{h,k-1}P^+_{h,k-1}A^T_{h,k-1} + Q_{h,k-1}$
  Symmetric positive definite matrice update: $\bar{S}_k = L_k^T S_k L_k$
- **Measurement update:**
  Kalman gain matrix update: $K_{h,k} = A_{h,k}P^-_{h,k}(I - \theta\bar{S}_k P^-_{h,k} + C^T_{h,k}R^{-1}_{h,k}C_{h,k}P^-_{h,k})^{-1}C^T_{h,k}R^{-1}_{h,k}$
  Update the posterior state: $\hat{x}^+_{h,k} = \hat{x}^-_{h,k} + K_{h,k}(y_k - C_{h,k}\hat{x}^-_{h,k} - D_{h,k}i_{o,k})$
  Update the posterior covariance of state:
  $P^+_{h,k} = P^-_{h,k}(I - \theta\bar{S}_k P^-_{h,k} + C^T_{h,k}R^{-1}_{h,k}C_{h,k}P^-_{h,k})^{-1} + R_{h,k}$
- **State vector output $x_{h,k}$ for SoC online estimation**

Table 3
Estimators for SoC estimation.

Estimator	Algorithm for state estimation	OCV-SoC relationship extracted from
Estimator (IO)	UKF	IO test
Estimator (LO)	UKF	LO test

(40 °C).

Fig. 3(D) illustrates the OCV-SoC curves of the incremental OCV test at various ambient temperatures and aging stages for LFP cells. The OCV-SoC curves at three temperatures of the new cell LFP01 only overlap in a small range of 50–70% SoC and have apparent differences in the other ranges. Compared with the new cell LFP01 at 10 °C, the OCV-SoC curve of the aged cell LFP09 has negligible differences in the range of 10–40% and 70–90% SoC. Unlike the incremental OCV test, the low current OCV-SoC curves as shown in Fig. 3(E) at three temperatures of the new cell LFP01 show more obvious wide flat in the range of 10–90% SoC. It is interesting to note that the OCV at high temperature (40 °C) is lower than those at the other two temperatures. Moreover, the OCV-SoC curves overlap substantially at room temperature (25 °C) for the new cell LFP01 and low temperature (10 °C) for the new cell LFP01 and aged cell LFP09 except for the high SoC region.

4. H_∞-UKF joint SoC estimation

4.1. H_∞ filter for parameters online identification

The ambient temperatures and aging stages not only affect the OCV-SoC relationship but also affect the battery parameters, so, the battery parameters (R_o, R_p and C_p) should be identified in real operating conditions to improve the SoC estimation accuracy. As H_∞ filter shows a better robustness performance to the noises and model error than the RLS algorithm. Besides, H_∞ filter can describe the working mechanism

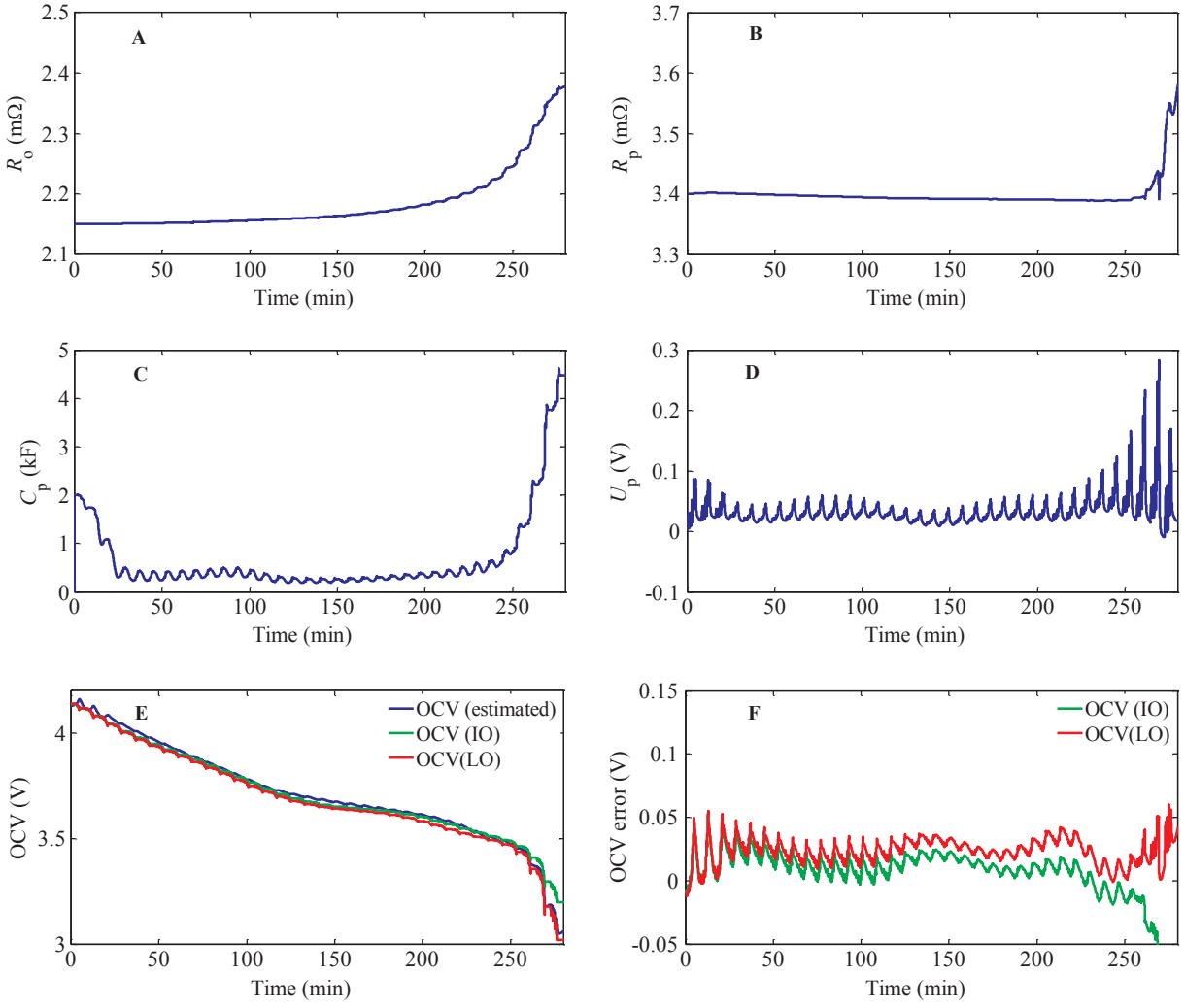

Fig. 4. Result of parameters identification for NMC01 at 25 °C: (A) R_o, (B) R_p, (C) C_p, (D) U_p, (E) OCV, (F) OCV error.

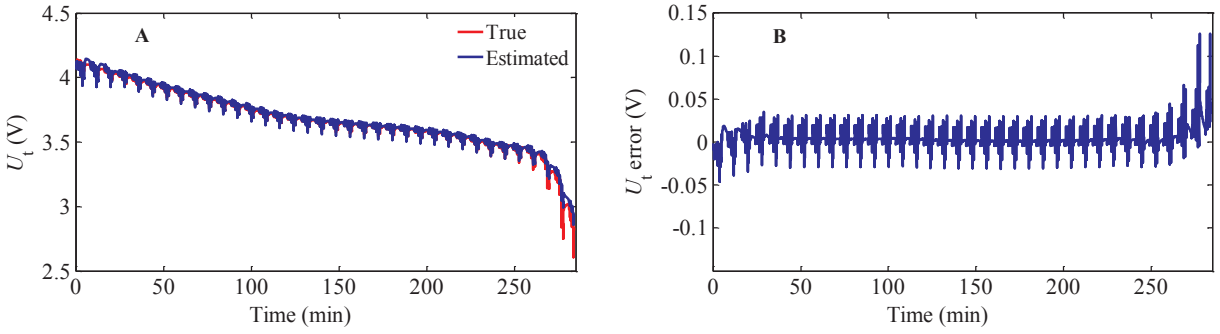

Fig. 5. Measured voltage and estimated voltage via H_∞ filter for the NMC01 cell at 25 °C: (A) U_t, (B): U_t error.

of the battery through the state-space equation. Therefore, in this paper, H_∞ filter is employed to update the parameters, and then the parameters are propagated to the state estimation process in real-time [28]. Notably, the OCV is identified as a parameter in the parameter identification process, which indicates that the two OCV tests only affect the SoC estimation process other than the parameters identification process, and it is more clearly to observe the impact of two OCV tests on SoC estimation. The state space equation for H_∞ filter is shown as follows:

$$\begin{cases} x_{h,k+1} = A_{h,k}x_{h,k} + B_{h,k}i_{o.k} + w_{h,k} \\ y_k = C_{h,k}x_{h,k} + D_{h,k}i_{o,k} + v_{h,k} \\ z_k = L_k x_{h,k} \end{cases} \quad (5)$$

where $x_{h,k}$ is the state and defined as $[OCV_k, U_{p,k}, C_{p,k}, R_{p,k}, R_{o,k}]^T$; y_k is the measurement and equals U_t, respectively; z_k is a linear combination of the state and defined as $[C_{p,k}, R_{p,k}, R_{o,k}]$, and L_k is a user-specified matrix according to z_k; u_k is the known input vector and equals $i_{o,k}$; $w_{h,k}$ and $v_{h,k}$ are the system white noise and measurement white noise, respectively. The matrices $C_{h,k}$ and $D_{h,k}$ are $[1, -1, 0, 0, -i_{o,k}]$ and $R_{o,k}$ respectively. The matrices $A_{h,k}$, $B_{h,k}$ and L_k are defined as follows:

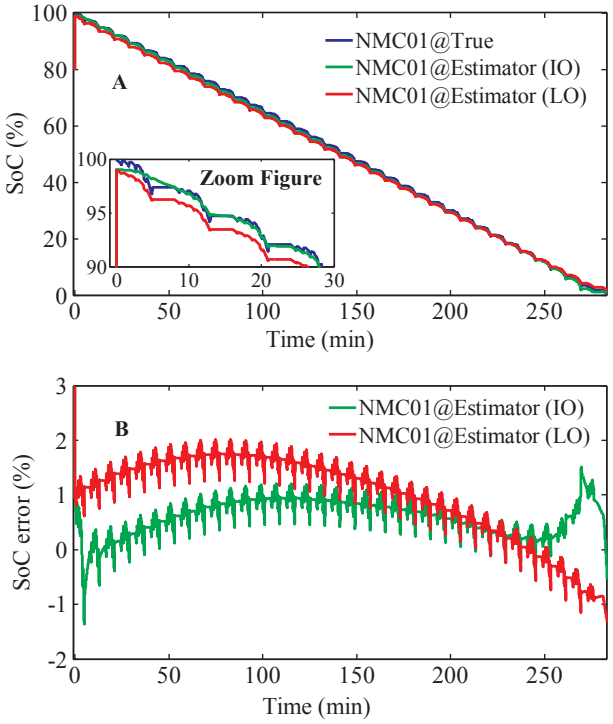

Fig. 6. Results of two estimators for NMC01 cell at 25 °C: (A) SoC, (B) SoC error.

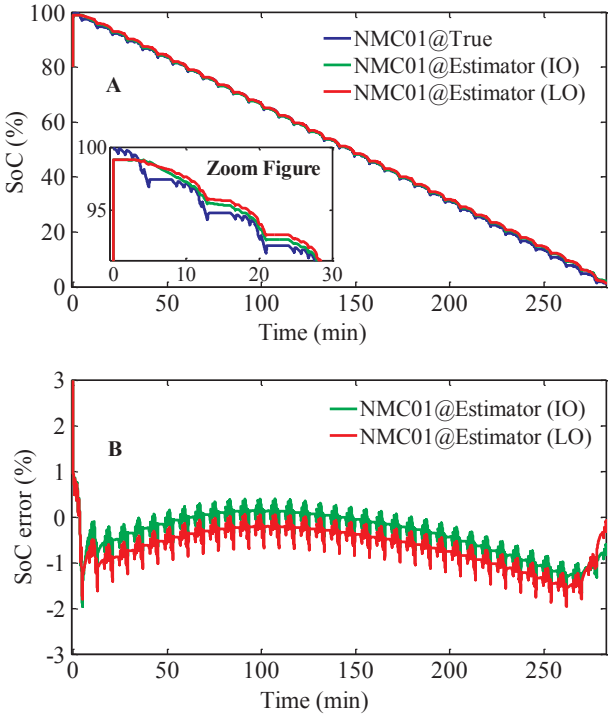

Fig. 7. Results of two estimators for NMC01 cell at 40 °C: (A) SoC, (B) SoC error.

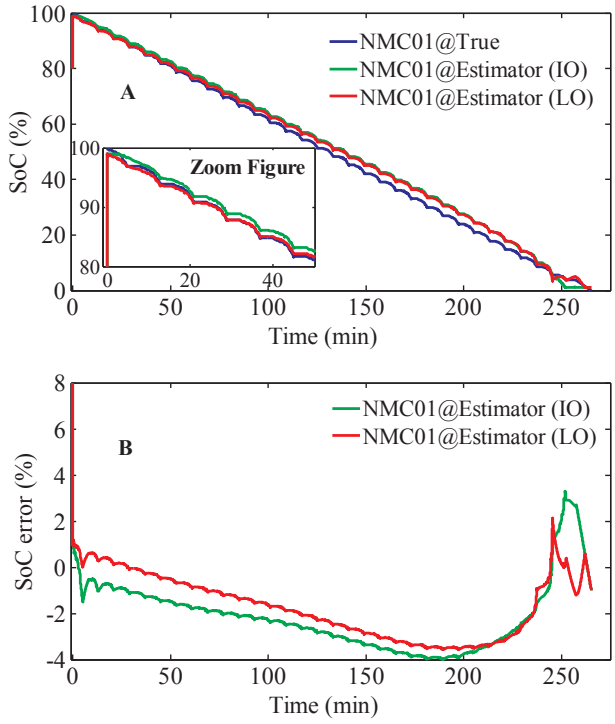

Fig. 8. Results of two estimators for NMC01 cell at 10 °C: (A) SoC, (B) SoC error.

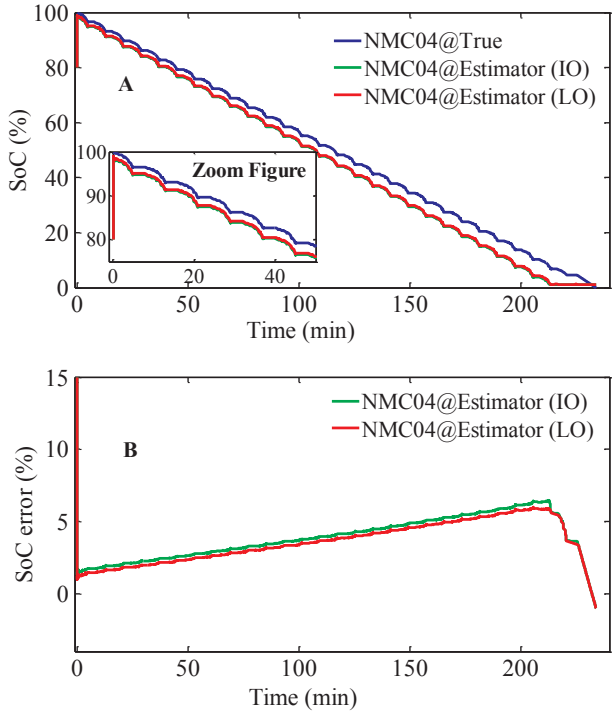

Fig. 9. Results of two estimators for NMC04 cell at 10 °C: (A) SoC, (B) SoC error.

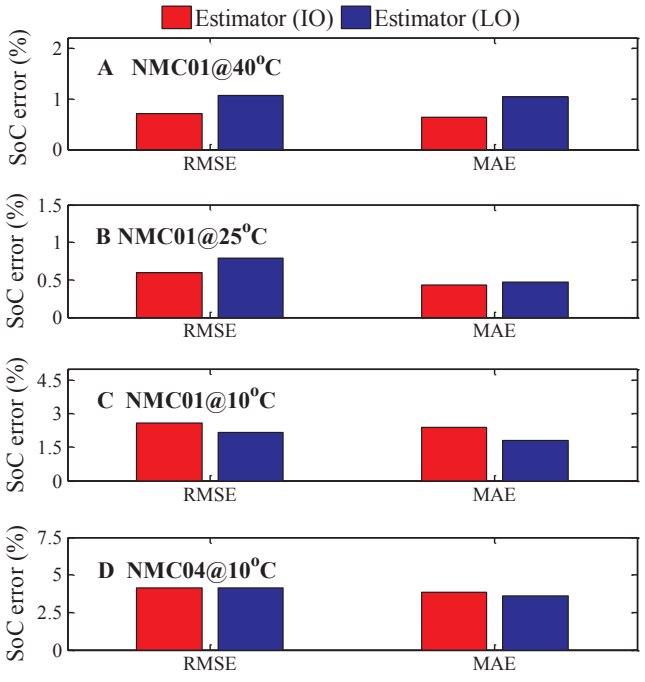

Fig. 10. Statistical indices of the SoC for NMC cells: (A) NMC01@40 °C, (B) NMC01@25 °C, (C) NMC01@10 °C, (D) NMC04@10 °C.

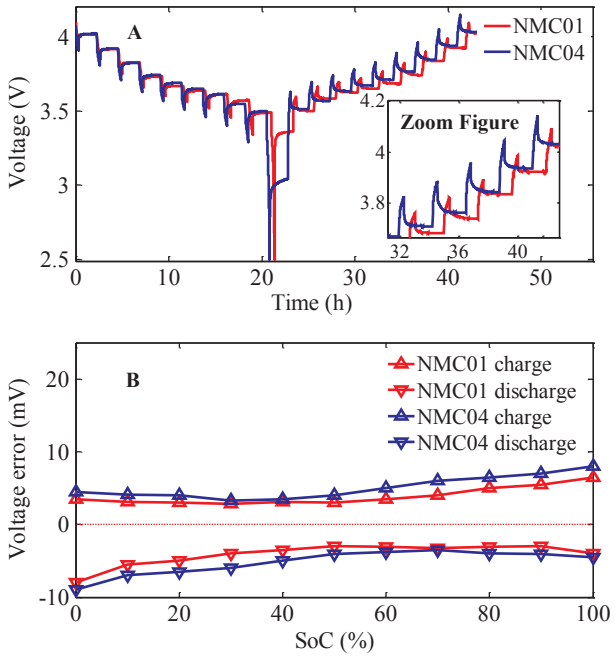

Fig. 11. The effect of rest time on OCV for NMC cells: (A) Voltage, (B) Voltage error.

$$\begin{cases} A_{h,k} = \begin{bmatrix} 1 & 0 & 0 & 0 & 0 \\ 0 & \theta_k & \frac{\Delta t}{C_{p,k}^2 R_{p,k}}\theta_k U_{p,k} & \left(\frac{\Delta t (U_{p,k}+R_p i_{o,k})}{C_{p,k}R_{p,k}^2} - i_{o,k}\right)\theta_k + i_{o,k} & 0 \\ 0 & 0 & 1 & 0 & 0 \\ 0 & 0 & 0 & 1 & 0 \\ 0 & 0 & 0 & 0 & 1 \end{bmatrix} \\ B_{h,k} = (1-\theta_k)R_p \\ L_k = \begin{bmatrix} 0 & 0 & 1 & 0 & 0 \\ 0 & 0 & 0 & 1 & 0 \\ 0 & 0 & 0 & 0 & 1 \end{bmatrix} \end{cases} \quad (6)$$

where $\theta = \exp(-\Delta t/C_p R_p)$.

The general process of the H_∞ filter for parameters identification is listed in Table 2.

4.2. UKF for SoC online estimation

Once the parameters of battery model identified at time kth. KF family filters often used to estimate the SoC. Compared with the KFs and EKFs, UKF shows better performances in robustness, computational speed, converge speed, and SoC estimation accuracy. Thus, in this paper, UKF is employed to estimate the SoC online, and the H_∞-UKF joint estimation method can update the parameters and estimate the states in real-time.

For the UKF filter, the state space equation can be formulated as:

$$\begin{cases} x_{u,k+1} = A_{u,k}x_{u,k} + B_{u,k}i_{o.k} + w_{u,k} \\ y_k = C_{u,k}x_{u,k} - D_{u,k}i_{o,k} + v_{u,k} \end{cases} \quad (7)$$

where $x_{u,k}$ is state and equals $[U_{p,k}, s_k]^T$; y_k is the measurement and defined as U_t;; u_k is the known input and defined as $i_{o,k}$; $w_{u,k}$ and $v_{u,k}$ are the system noise and measurement noise, respectively. The matrices in Eq. (7) are defined as:

$$\begin{cases} A_{u,k} = \begin{bmatrix} 1-\theta_k & 0 \\ 0 & 1 \end{bmatrix} \\ B_{u,k} = \begin{bmatrix} (1-\theta_k)R_p \\ \eta_i \Delta t / C_n \end{bmatrix} \\ C_{h,k} = \begin{bmatrix} -1 & \frac{dOCV}{dSoC} \end{bmatrix} \\ D_{h,k} = R_{o,k} \end{cases} \quad (8)$$

Then we could use UKF to estimate the SoC with Eqs. (7) and (8), and the general process of UKF for SoC estimation can be referred to [14].

5. Results and discussion

With the parameters identified via H_∞ filter in real-time, two estimators are defined in Table 3 to observe the impact of two OCV tests on the SoC online estimation at various temperatures and aging stages. To verify the H_∞-UKF joint estimation method, the typical the dynamic stress test (DST) is employed in this study. For the battery cells, the initial SoC is 100% when it's fully charged, but it's difficult to obtain an accurate initial SoC value in real applications, thus, it is assumed that the initial SoC is set to 80% (with 20% initial error) to verify the robustness of the H_∞-UKF joint estimation method. In addition, the statistical indices such as root mean square error (RMSE) and mean absolute error (MAE) as shown in Eq. (9) are used to assess the performance of the H_∞-UKF joint estimation method.

$$\text{RMSE} = \sqrt{\frac{1}{n}\sum_{k=1}^{n} |s_{a,k} - s_{u,k}|^2}, \quad MAE = \frac{1}{n}\sum_{k=1}^{n} |s_{a,k} - s_{u,k}| \quad (9)$$

where $s_{a,k}$ is the true SoC calculated from the Ampere-hour counting method via the high precision current sensor in Arbin BT2000 battery test machine; $s_{u,k}$ is the estimated SoC by the H_∞-UKF joint estimation method.

5.1. Experimental results and discussion for NMC lithium-ion cells

The result of parameters identification through H_∞ filter at 25 °C under DST test for the new cell NMC01 is shown in Fig. 4. Fig. 4(A)-(D) represent the battery's ohmic resistance Ro, polarization resistance R_p, polarization capacitance C_p and voltage U_p, respectively. Fig. 4(E) indicates the OCV curves, the blue curve is the estimated OCV via H_∞ filter, the green curve is the OCV predetermined by IO test while the red curve is the OCV predetermined by LO test.

Fig. 5(F) depicts that there are only small differences between the

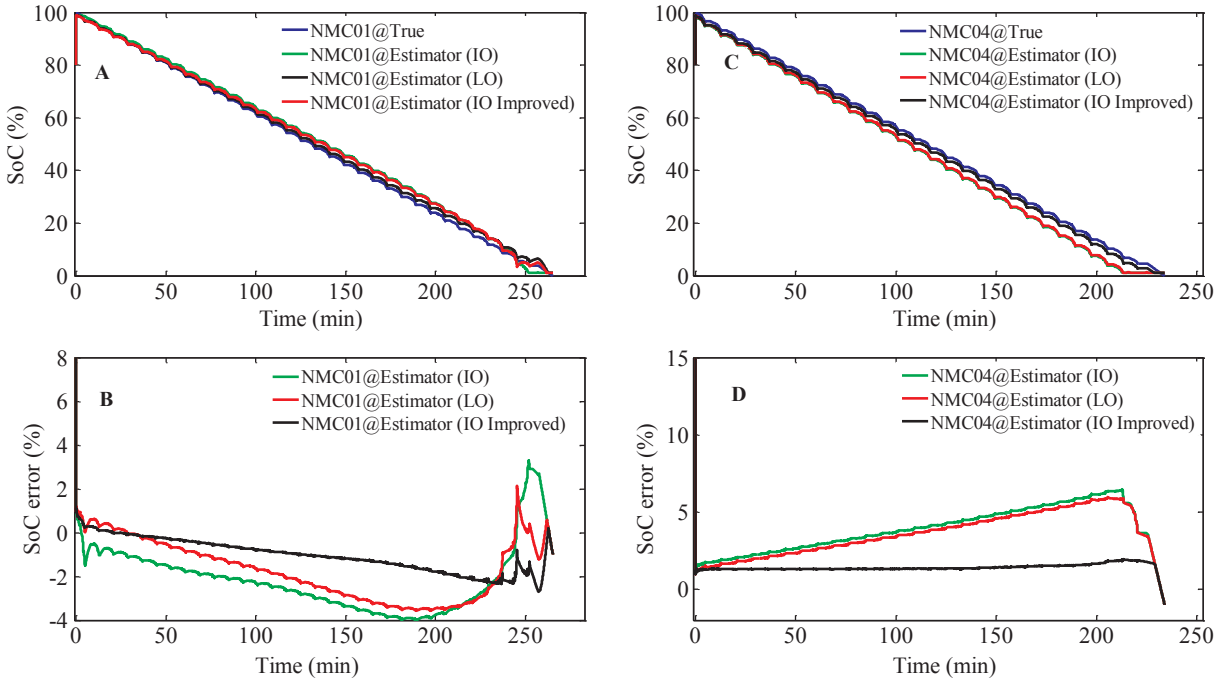

Fig. 12. Comparison of three estimators for NMC cells under DST test at 10 °C: (A) SoC for NMC01, (B) SoC error NMC01, (C) SoC NMC04, (D) SoC error NMC04.

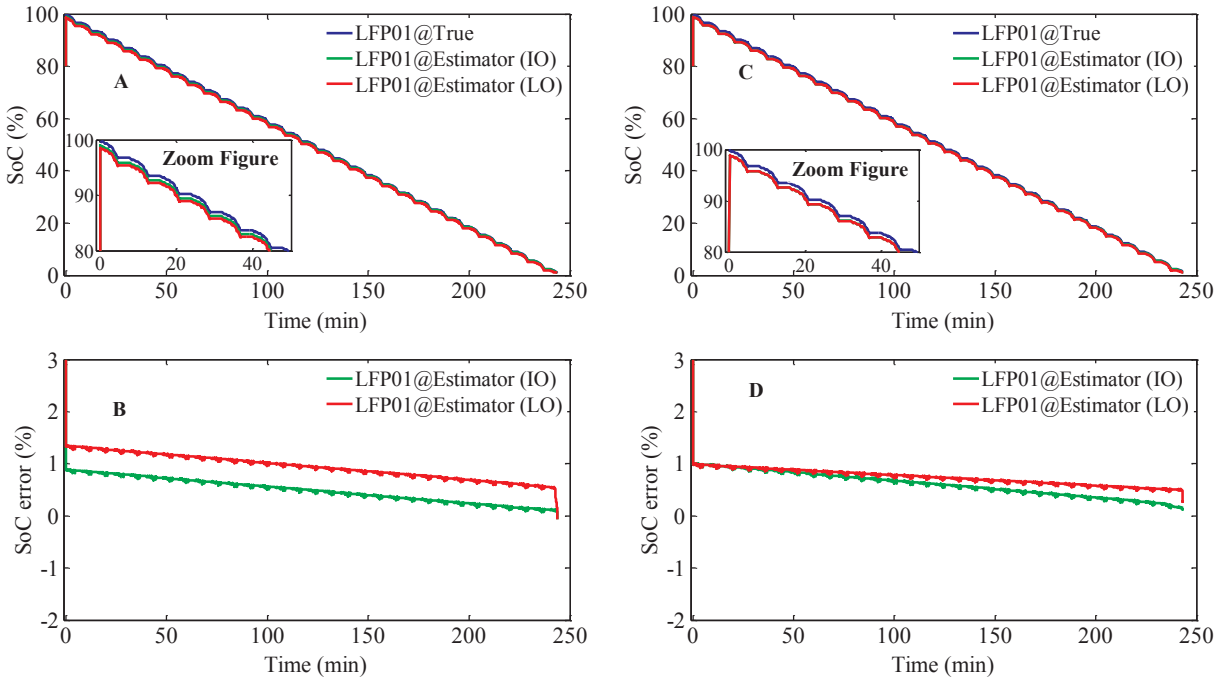

Fig. 13. Results of two estimators for LFP01 cell at 40 °C and 25 °C: (A) SoC at 40 °C, (B) SoC error at 40 °C, (C) SoC at 25 °C, (D) SoC error at 25 °C.

OCV (IO), OCV (LO) and the estimated OCV. Moreover, the estimated OCV is closer to the IO test than LO test. The measured voltage and estimated voltage are illustrated in Fig. 5(A), and the voltage error is shown in Fig. 5(B). The voltage error is less than 0.05 V except for the end of the discharge, which may be caused by the large model error at low SoC region.

Fig. 6(A) shows the results of the H_∞-UKF joint estimation method at 25 °C and Fig. 6(B) depicts the corresponding SoC errors. Both the two estimators can converge to the true SoC quickly when the initial SoC are inaccurately initialized, and the estimator (IO) performs better than the estimator (LO) at the whole testing time. Furthermore, the maximum SoC errors of both two estimators are smaller than 2% at the whole discharge process.

The comparison results between the two estimators at 40 °C are shown in Fig. 7. The results reveal that both estimators perform well in terms of convergence time and SoC errors at 40 °C, but the estimator (IO) is relative better in terms of SoC error, which indicates the estimator (IO) based on the OCV-SoC relationship predetermined by incremental OCV test can provide a higher accuracy than the estimator (LO) based on the OCV-SoC relationship predetermined by low current OCV test.

At 10 °C, a new cell NMC01 and an aged cell NMC04 are tested with DST cycles, and the results of two estimators are shown in Figs. 8 and 9 respectively. For the new cell, although the two estimators can

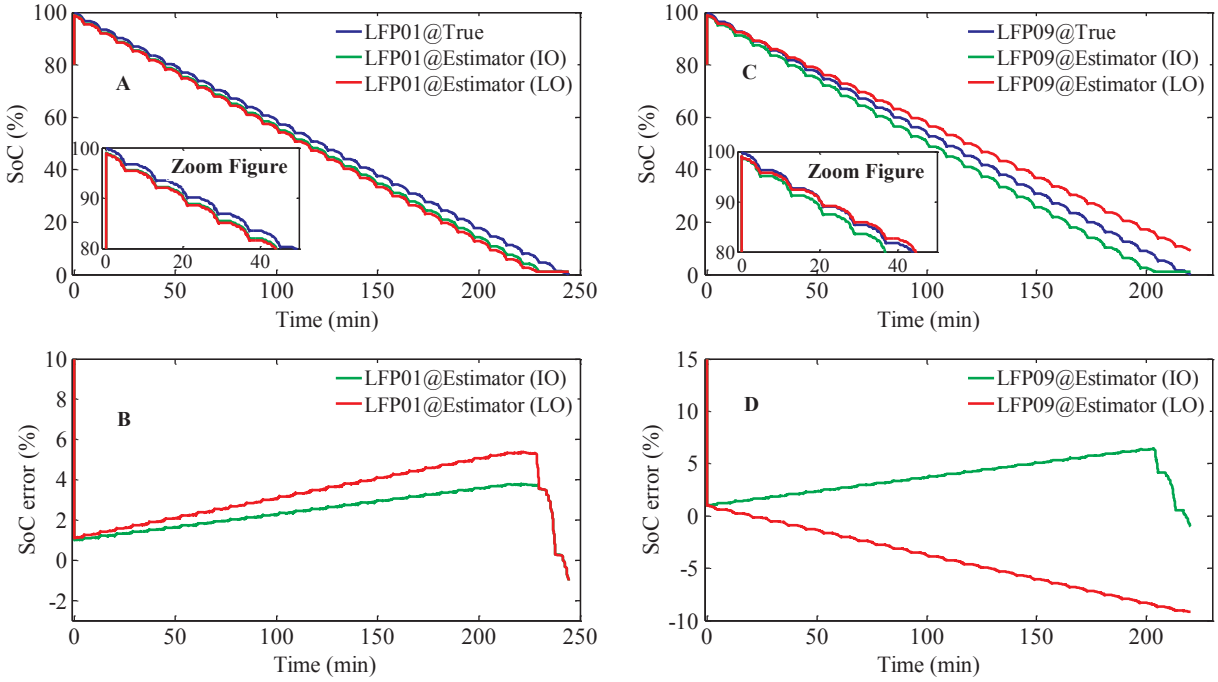

Fig. 14. Results of two estimators for LFP01 and LFP09 cell at 10 °C: (A) SoC for LFP01, (B) SoC error for LFP01, (C) SoC for LFP09, (D) SoC error for LFP09.

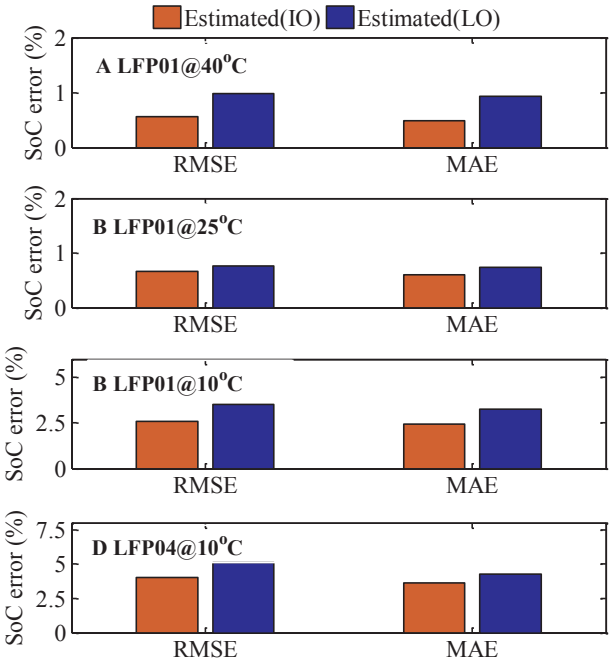

Fig. 15. Statistical indices of the SoC for LFP cells: (A) LFP01@40 °C, (B) LFP01@25 °C, (C) LFP09@10 °C, (D): LFP09@10 °C.

converge to the true SoC very fast, the SoC errors increase gradually except for the end of discharge. It's interesting that the estimator (LO) performs slight better than estimator (IO). For the aged cell, the same conclusions can be drawn. Consequently, we can conclude that the estimator (LO) performs better than estimator (IO) for these two cells at 10 °C.

As shown in Fig. 10, the estimator (IO) outperforms estimator (LO) for the new cell at 40 °C and 25 °C. However, when the temperature decreases to 10 °C, the estimator (LO) performs better than estimator (IO). The large SoC errors at 10 °C may be caused by the inaccuracy of the OCV-SoC due to the short relaxation time.

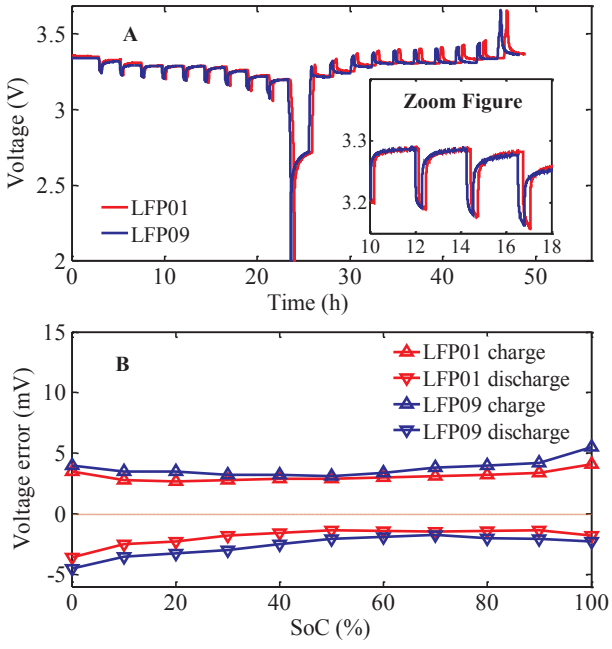

Fig. 16. The effect of rest time on OCV for LFP cells: (A) Voltage, (B) Voltage error.

Fig. 11(A) shows that the voltage profiles of incremental OCV test for NMC01 and NMC04 at 10 °C. It's clear that the voltages are not stable at some SoC levels, which indicates that the polarization effect still exist inside the cell at the low temperature and needs more relaxation time to eliminate it. Then we extend the relaxation period from 2 h to 3 h at 10 °C, the voltage errors between the improved incremental OCV test (the relaxation period is 3 h) and incremental OCV test (the relaxation period is 2 h) are shown in Fig. 11(B). The impact of three OCV tests on SoC estimation at 10 °C is illustrated in Fig. 12, the results reveal that the estimator (IO improved) performs better than the estimator (IO) and the estimator (LO), which indicates that it's necessary to extend the relaxation time to eliminate the polarization effect and improve the SoC accuracy for NMC LiBs at low temperatures.

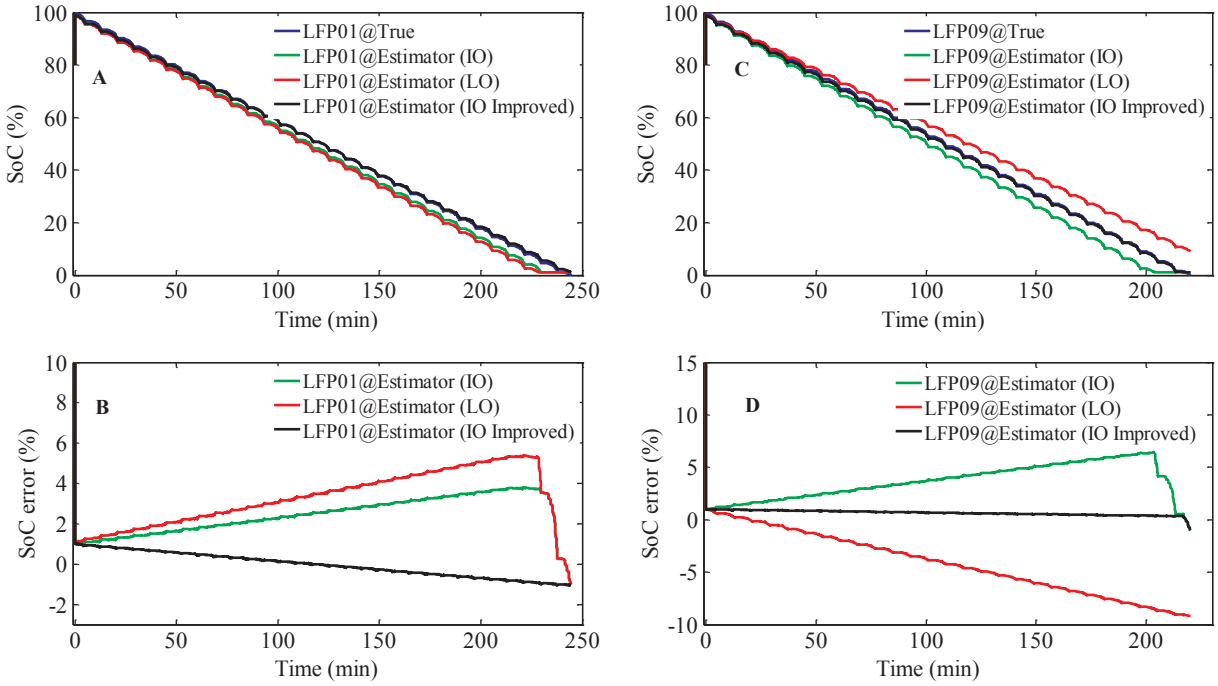

Fig. 17. Comparison of three estimators for LFP cells test at 10 °C: (A) SoC for LFP01, (B) SoC error LFP01, (C) SoC LFP09, (D) SoC error LFP09.

As discussed above, the estimator (IO) performs better than the estimator (LO) for NMC LiBs. therefore, this study recommends the incremental OCV test to determine the OCV-SoC relationship for NMC LiBs, however, the relaxation period should extend from 2 h to 3 h or much longer at low temperatures, the relaxation period can be fixed through the impedance test.

5.2. Experimental results and discussion for LFP lithium-ion cells

Unlike the NMC LiBs, the OCV-SoC curves of LFP LiBs usually have a typical wide flat platform and change dramatically in the low and high SoC regions, hence, it also needs to analyse the impact of two OCV tests on LFP LiBs' SoC online estimation.

Fig. 13(A) describes that the results of two estimators for the new cell LFP01 at 40 °C, the corresponding SoC errors are shown in Fig. 13(B). The maximum SoC errors of two estimators are below 1.5%. Fig. 13(C) depicts the results of two estimators for LFP01 at 25 °C, the corresponding SoC errors are illustrated in Fig. 13(D). The maximum SoC errors of two estimators are below 1%. In addition, the estimator (IO) performs better than estimator (LO) for LFP01 at 40 °C and 25 °C.

Fig. 14(A) shows that the results of two estimators for the new cell LFP01 at 10 °C, the corresponding SoC errors are illustrated in Fig. 14(B). Although both estimators perform worse at 10 °C than that at 40 °C and 25 °C, the estimator (IO) performs better than estimator (LO) for LFP01 at 10 °C. Fig. 14(C) depicts the results of two estimators for the aged cell LFP09 at 10 °C, the corresponding SoC errors are shown in Fig. 14(D). It's clear that the SoC errors of both estimators for the aged cell LFP09 at 10 °C are larger than that for the new cell LFP01 at 10 °C. However, the estimator (IO) performs better than estimator (LO) for LFP09 at 10 °C. Therefore, the estimator (IO) performs better than estimator (LO) for the two aging stages LFP LiBs at 10 °C.

Like the NMC LiBs, the statistical indices of the SoC results for LFP LiBs are illustrated in Fig. 15. The estimator (IO) performs better than estimator (LO) for the new cell LFP01 at 40 °C and 25 °C. When the temperature decreases to 10 °C, the SoC errors of both estimators for LFP01 and LFP09 are larger than that at 40 °C and 25 °C. The large SoC errors at 10 °C may also be caused by the inaccuracy of the OCV-SoC due to the short relaxation time. Fig. 16(A) shows that the voltage profiles of incremental OCV tests for LFP01 and LFP09 at 10 °C. It's clear that the voltages are not stable at some SoC levels, which indicates that the polarization effect still exist inside the cell at the low temperature and needs more relaxation time to eliminate it. Then we extend the relaxation period from 2 h to 3 h at low temperature, the voltage error between the improved incremental OCV test (the relaxation period is 3 h) and incremental OCV test (the relaxation period is 2 h) at 10 °C is shown in Fig. 16(B). The impact of three OCV tests on SoC estimation for LFP cells at 10 °C is illustrated in Fig. 17, the results reveal that the estimator (IO improved) performs batter than the estimator (IO) and the estimator (LO), which indicates that it's necessary to extend the relaxation time to eliminate the polarization and improve the SoC accuracy for LFP cell at low temperatures.

As discussed above, the estimator (IO) performs batter than the estimator (LO) for LFP LiBs. therefore, this study recommends the incremental OCV test to determine the OCV-SoC relationship for LFP LiBs, however, the relaxation period should extend from 2 h to 3 h at low temperatures, otherwise, the obtained OCV profiles may not be in an equilibrium state.

6. Conclusions

The accurate OCV-SoC relationship is essential to improve battery SoC estimation accuracy in practical applications. The incremental OCV test and low current OCV test are the two commonly approaches used to determine the relationship of OCV-SoC. The temperatures and aging stages often affect the OCV-SOC curve, hence, the impact of these two OCV tests on SoC online estimation at three ambient temperatures and two aging stages for NMC and LFP LiBs are investigated. The SoC is estimated via an H_∞-UKF joint estimation method which is proposed to update the parameters and estimate SoC in real-time. The proposed method is verified at different temperatures and aging stages. As H_∞ filter can identify OCV as a parameter during parameter identification operation, then the two OCV tests only affect the SoC estimation process, therefore, it's more clearly to study the impact of two OCV tests on SoC estimation. The study results show that the incremental OCV test performs better than low current OCV test for both NMC and LFP LiBs, however, the relaxation time needs to be taken into consideration for

incremental OCV tests, especially at low temperatures. This paper recommends the OCV test to determine the relationship of OCV-SoC for both NMC and LFP cells. The relaxation period can be set to 2 h at room temperature (25 °C) and high temperature (40 °C), but the rest time should be extended from 2 h to a much longer period at low temperature (10 °C).

Due to the laboratory conditions and time constraints, the impact of two OCV tests on SoC online estimation method only studied at three temperatures are two aging states at 10 °C. There are a lot of work to be done in our future work, for example, the rest time for incremental OCV test will be conducted at more temperatures below room temperature to determine the proper rest time at various temperatures for NMC and LFP LiBs. In addition, the rest time will be conducted at more aging stages to obtain the proper rest time at various aging sages for NMC and LFP aged cells.

Acknowledgements

This work was supported by the National Natural Science Foundation of China (Grant No. 51507012) and Beijing Nova Program (Grant No. Z171100001117063). The systemic experiments of the lithium-ion batteries were performed at the Advanced Energy Storage and Application (AESA) Group, Beijing Institute of Technology.

References

[1] Dong G, Wei J, Zhang C, Chen Z. Online state of charge estimation and open circuit voltage hysteresis modeling of LiFePO4 battery using invariant imbedding method. Appl Energy 2016;162:163–71.
[2] Barai A, Widanage WD, Marco J, Mcgordon A, Jennings P. A study of the open circuit voltage characterization technique and hysteresis assessment of lithium-ion cells. J Power Sources 2015;295:99–107.
[3] Jaguemont J, Boulon L, Dubé Y. A comprehensive review of lithium-ion batteries used in hybrid and electric vehicles at cold temperatures. Appl Energy 2016;164:99–114.
[4] Xiong R, Zhang Y, He H, Zhou X. Michael Pecht, A double-scale, particle-filtering, energy state prediction algorithm for lithium-ion batteries. IEEE Trans Ind Electron 2017. http://dx.doi.org/10.1109/TIE.2017.2733475.
[5] Chang W-Y. The state of charge estimating methods for battery: a review. ISRN Appl Math 2013;2013:1–7.
[6] Piller S, Perrin M, Jossen A. Methods for state-of-charge determination and their applications. J. Power Sources 2001;96:113–20.
[7] Zou Y, Hu X, Ma H, Li SE. Combined state of charge and state of health estimation over lithium-ion battery cell cycle lifespan for electric vehicles. J Power Sources 2015;273:793–803.
[8] Yanhui Z, Wenji S, Shili L, Jie L, Ziping F. A critical review on state of charge of batteries. J Renew Sustain Energy 2013;5:93–110.
[9] Pop V, Bergveld HJ, Notten PHL, Regtien PPL. State-of-the-art of battery state-of-charge determination. Meas Sci Technol 2005;16:R93–110.
[10] Xing Y, He W, Pecht M, Tsui KL. State of charge estimation of lithium-ion batteries using the open-circuit voltage at various ambient temperatures. Appl Energy 2014;113:106–15.
[11] Xiong R, Tian JP, Mu H, Wang C. A systematic model-based degradation behavior recognition and health monitor method of lithium-ion batteries. Appl Energy 2017. http://dx.doi.org/10.1016/j.apenergy.2017.05.124.
[12] Di Domenico D, Fiengo G, Stefanopoulou A. Lithium-ion battery state of charge estimation with a Kalman Filter based on a electrochemical model. Control Appl 2008 CCA 2008 IEEE Int Conf; 2008. p. 702–7.
[13] Di Domenico D, Stefanopoulou A, Fiengo G. Lithium-Ion battery state of charge and critical surface charge estimation using an electrochemical model-based extended Kalman filter. J Dyn Syst Meas Control 2010;132:768–78.
[14] Yu Q, Xiong R, Lin C, Shen WX, Deng JJ. Lithium-ion battery parameters and state-of-charge joint estimation based on H infinity and unscented kalman filters. IEEE Trans Veh Technol 2017. http://dx.doi.org/10.1109/TVT.2017.2709326.
[15] Zheng WX. Estimation of the parameters of autoregressive signals from colored noise-corrupted measurements. IEEE Signal Process Lett 2000;7:201–4.
[16] Zhao X, de Callafon RA. Modeling of battery dynamics and hysteresis for power delivery prediction and SOC estimation. Appl Energy 2016;180:823–33.
[17] Wei Z, Meng S, Xiong B, Ji D, Tseng KJ. Enhanced online model identification and state of charge estimation for lithium-ion battery with a FBCRLS based observer. Appl Energy 2016;181:332–41.
[18] Gao J, Zhang Y, He H. A real-time joint estimator for model parameters and state of charge of lithium-ion batteries in electric vehicles. Energies 2015;8:8594–612.
[19] Wei Z, Zhao J, Ji D, Tseng KJ. A multi-timescale estimator for battery state of charge and capacity dual estimation based on an online identified model. Appl Energy 2017.
[20] Dai H, Xu T, Zhu L, Wei X, Sun Z. Adaptive model parameter identification for large capacity Li-ion batteries on separated time scales. Appl Energy 2016;184:119–31.
[21] Zheng L, Zhang L, Zhu J, Wang G, Jiang J. Co-estimation of state-of-charge, capacity and resistance for lithium-ion batteries based on a high-fidelity electrochemical model. Appl Energy 2016;180:424–34.
[22] Xiong R, Sun F, Chen Z, He H. A data-driven multi-scale extended Kalman filtering based parameter and state estimation approach of lithium-ion olymer battery in electric vehicles. Appl Energy 2014;113:463–76.
[23] Guo X, Kang L, Yao Y, Huang Z, Li W. Joint estimation of the electric vehicle power battery state of charge based on the least squares method and the Kalman filter algorithm. Energies 2016;9:1–16.
[24] Wang Y, Zhang C, Chen Z. A method for state-of-charge estimation of LiFePO4 batteries at dynamic currents and temperatures using particle filter. J Power Sources 2015;279:306–11.
[25] Yan J, Xu G, Xu Y. Battery state-of-charge estimation based on H-infinity filter for hybrid electric vehicle. In: Proc. 2008 10th Int. Conf. Control. Autom. Robot. Vis.; 2008. p. 464–9.
[26] Charkhgard M, Zarif MH. Design of adaptive H∞ filter for implementing on state-of-charge estimation based on battery state-of-charge-varying modelling. IET Power Electron 2015;8:1825–33.
[27] Aung H, Soon Low K, Ting Goh S. State-of-charge estimation of lithium-ion battery using square root spherical unscented Kalman filter (Sqrt-UKFST) in nanosatellite. IEEE Trans Power Electron 2015;30:4774–83.
[28] Xiong R, Yu Q, Wang LY, Lin C. A novel method to obtain the open circuit voltage for the state of charge of lithium ion batteries in electric vehicles by using H infinity filter. Appl Energy 2017. http://dx.doi.org/10.1016/j.apenergy.2017.05.136.
[29] Truchot C, Dubarry M, Liaw BY. State-of-charge estimation and uncertainty for lithium-ion battery strings. Appl Energy 2014;119:218–27.
[30] Marongiu A, Nußbaum FGW, Waag W, Garmendia M, Sauer DU. Comprehensive study of the influence of aging on the hysteresis behavior of a lithium iron phosphate cathode-based lithium ion battery - an experimental investigation of the hysteresis. Appl Energy 2016;171:629–45.
[31] Wang S, Shang L, Li Z, Deng H, Li J. Online dynamic equalization adjustment of high-power lithium-ion battery packs based on the state of balance estimation. Appl Energy 2016;166:44–58.
[32] Pei L, Wang T, Lu R, Zhu C. Development of a voltage relaxation model for rapid open-circuit voltage prediction in lithium-ion batteries. J Power Sources 2014;253:412–8.
[33] Pattipati B, Balasingam B, Avvari GV, Pattipati KR, Bar-Shalom Y. Open circuit voltage characterization of lithium-ion batteries. J Power Sources 2014;269:317–33.
[34] Matsui H, Nakamura T, Kobayashi Y, Tabuchi M, Yamada Y. Open-circuit voltage study on LiFePO4 olivine cathode. J Power Sources 2010;195:6879–83.
[35] Lavigne L, Sabatier J, Francisco JM, Guillemard F, Noury A. Lithium-ion Open Circuit Voltage (OCV) curve modelling and its ageing adjustment. J Power Sources 2016;324:694–703.
[36] Xia B, Chen C, Tian Y, Wang M, Sun W, Xu Z. State of charge estimation of lithium-ion batteries based on an improved parameter identification method. Energy 2015;90:1426–34.
[37] Roscher MA, Sauer DU. Dynamic electric behavior and open-circuit-voltage modeling of LiFePO 4-based lithium ion secondary batteries. J Power Sources 2011;196:331–6.
[38] Cheng KWE, Divakar BP, Wu H, Ding K, Ho HF. Battery-management system (BMS) and SOC development for electrical vehicles. IEEE Trans Veh Technol 2011;60:76–88.
[39] Chen Z, Member A, Fu Y, Mi CC. State of charge estimation of lithium-ion batteries in electric drive vehicles using extended Kalman filtering. IEEE Trans Veh Technol 2013;62:1020–30.
[40] Nejad S, Gladwin DT, Stone DA. A systematic review of lumped-parameter equivalent circuit models for real-time estimation of lithium-ion battery states. J Power Sources 2016;316:183–96.
[41] Weng C, Sun J, Peng H. A unified open-circuit-voltage model of lithium-ion batteries for state-of-charge estimation and state-of-health monitoring. J Power Sources 2014;258:228–37.
[42] Zheng F, Xing Y, Jiang J, Sun B, Kim J, Pecht M. Influence of different open circuit voltage tests on state of charge online estimation for lithium-ion batteries. Appl Energy 2016;183:513–25.
[43] Sun F, Xiong R, He H. A systematic state-of-charge estimation framework for multi-cell battery pack in electric vehicles using bias correction technique. Appl Energy 2016;162:1399–409.